

RSC Advances



This is an *Accepted Manuscript*, which has been through the Royal Society of Chemistry peer review process and has been accepted for publication.

Accepted Manuscripts are published online shortly after acceptance, before technical editing, formatting and proof reading. Using this free service, authors can make their results available to the community, in citable form, before we publish the edited article. This *Accepted Manuscript* will be replaced by the edited, formatted and paginated article as soon as this is available.

You can find more information about *Accepted Manuscripts* in the [Information for Authors](#).

Please note that technical editing may introduce minor changes to the text and/or graphics, which may alter content. The journal's standard [Terms & Conditions](#) and the [Ethical guidelines](#) still apply. In no event shall the Royal Society of Chemistry be held responsible for any errors or omissions in this *Accepted Manuscript* or any consequences arising from the use of any information it contains.

Introduction of α -MnO₂ nanosheets to NH₂-graphene to remove Cr⁶⁺ from aqueous solutions

Li Zhang,^a Yaxi Tian,^a Yaopeng Guo,^a Hui Gao,^b Haizhen Li^a and Shiqiang Yan*

Abstract: The planar structure of the designed α -MnO₂-NH₂-RGO hybrid were prepared and characterized and used to remove hexvalent chromium ions (Cr⁶⁺) in aqueous solution. The characterization of the novel adsorbent was carried out using the Fourier transform infrared spectrum (FTIR), X-ray diffraction (XRD), Transmission electron microscope (TEM), Brunauer-Emmett-Teller (BET). The Cr⁶⁺ adsorption efficiency was investigated as a function of the pH of Cr⁶⁺ solution, contact time and temperature. The results exhibited that the adsorption capacity depended on the pH strongly and the adsorption equilibrium data were best described by the Freundlich isothermal model. The maximum sorption capacity towards Cr⁶⁺ was 371 mg/g. The kinetic adsorption was fitted to the pseudo-second-order kinetics model indicated that the adsorption mechanism is physical and chemical sorption on heterogeneous materials. The thermodynamic parameters were obtained and the results showed that the process of adsorption is spontaneous and exothermic. The adsorption capacity of α -MnO₂-NH₂-RGO can remain up to 81% after five cycles of usage. Consequently, the findings propose that α -MnO₂-NH₂-RGO could be used as an outstanding adsorbent for Cr⁶⁺.

Key words Chromium Graphene Manganese dioxide Adsorption

1. Introduction

Chromium has been considered to be one of the most common pollutants because of its wide spread use in industrial processes[1]. The use of chromium in pigment manufacture, leather tanning, metal finishing, ink manufacturing, automobile spare parts are the main sources of chromium based pollution. The acute toxicity, mutagenicity and carcinogenicity of chromium are strongly dependent on the oxidation state[2]. Chromium exists in the environment in both trivalent[Cr(III)] (Cr^{3+}) and hexavalent[Cr(VI)] (Cr^{6+}) forms. However, the hexavalent chromium Cr^{6+} is more toxic and more mobile in nature than trivalent[Cr(III)]. Because of unbiodegradation and easy accumulation in living beings[3], it can cause various diseases and disorder generating fatal effects, such as corrosion of skin, respiratory tract, lung carcinoma, severe diarrhea, and hemorrhage, etc.[4] The World Health Organization (WHO) recommends a maximum allowable level of 50 ppb total chromium for drinking water. The US Environmental Protection Agency established a guideline of 100 ppb maximum contaminant level for total chromium in drinking water[5,3].

To meet environmental regulations, effluents or water polluted with chromium must be treated before discharge. The technologies available for controlling Cr^{6+} in the environment include ion exchange[6], chemical precipitation[7], reverse osmosis[8], and adsorption[4]. Adsorption is considered as attractive and cost-effective method for removal recovery and recycling of metals from wastewater. The biosorbents can adequately remove heavy metal ions, they don't show mechanical strength because of low selectivity[9]. As for the chemical reduction precipitation process, the hexavalent chromium is reduced to the trivalent chromium[10]. However, this process is high-cost and the treatment is not completely and the water still has high Cr^{6+} concentration. These defects have improved the applications for Cr^{6+} removal from effluents or wastewater. Thus, it is a pressing need to develop new materials with high specific surface area, high adsorption capacity, easy sorption and stability in extreme conditions[11].

Being a one-atom-thick sheet of carbon atoms packed in two-dimensional (2D) honeycomb lattices, graphene possesses large theoretical specific surface area ($2630 \text{ m}^2/\text{g}$)[12], superior electronic and outstanding chemical stability[13]. Nowadays, the significant attention for graphene has been enjoyed on the preparation of graphene-based composites because it is an outstanding support[14,15]. Among these nanocomposites, considerable attention has been drawn on integrating graphene with other inorganic particles to fabricate composites or hybrids. In brief, it is believed that adhesion of inorganic materials to graphene can prevent the graphene sheets from aggregating and keep the specific surface area and pore volume at a high level, which is essential for applications such as adsorption processes and photocatalysis. On the other hand, the graphene can efficiently stabilize inorganic particles to prevent their aggregation, and the performance of these inorganic materials could be enhanced through loading on the graphene[16,17,18,19].

Recent studies have showed that oxide minerals, ubiquitous in soils, rocks and sediments, serve as natural sinks for contaminants in the environment[20,21]. Nanosized manganese oxide (MnO_2) are among the most reactive minerals that have a large specific surface area, outstanding oxidizing/adsorption abilities, and excellent stability under acidic conditions[22]. It provides an effective scavenging pathway for heavy metals in poisonous systems.

In general, the surface charge of MnO_2 is negative, and they can be used as dominant adsorbents to remove heavy metals from water effluents. However, as the medium of filtration, pure manganese oxide is uneconomical and disadvantageous and physical characteristic that MnO_2 attenuates numerous heavy metal ions via adsorption, ion exchange, co-precipitation. Thus, it is highly desirable to explore the support of the MnO_2 that can increase the removal efficiency for heavy ions with a low cost and environmentally benign nature[23].

In the present work, we demonstrate a novel hybrid nanostructure consist of distinct ultrathin nanosheets for greatly enhanced the adsorption performance. Partially, the structures based on the $\alpha\text{-MnO}_2$ nanosheets integrated on NH_2 -graphene sheets can introduce more active adsorption sites and bring extra interface at the hybridized

interlayer areas to promote adsorption process. Meanwhile, the α -MnO₂ integrated on NH₂-graphene can potentially tailor the distance between each layer of densely stacked graphene and open up the interlayer space to allow for more Cr⁶⁺ ions to adsorb effectively into the hybridized film. Consequently, the hybrid nanostructure design may enhance the adsorption of Cr⁶⁺, because it enlarges the specific surface area and improves the distribution channel of graphene. Hierarchically structured α -MnO₂-NH₂-RGO is obtained by chemically integrating α -MnO₂ nanosheets on NH₂-graphene because of the strong electrostatic interaction in the process solution treatment. It is evidenced that the water-exfoliated δ -MnO₂ nanosheet is electronegative and DMF-exfoliated NH₂-graphene is electropositive. The produced composite was characterized by Fourier transform infrared spectrum (FTIR), X-ray diffraction (XRD), Transmission electron microscope (TEM), Brunauer-Emmett-Teller (BET). To evaluate the adsorption behaviors further, the pH of Cr⁶⁺ solution, contact time and temperature were studied. In addition, the adsorption kinetics model, rate-limiting mechanism and the thermodynamics of the hybrids were also examined.

2. Experimental

2.1 Materials

Natural flake graphite was obtained from Nanyang Boxing mining Co., Ltd. (China). Other chemicals (analytical grade) were purchased from AiHua Fine Chemicals Co.,Ltd. (China), and use as received without any further purification.

2.2 Preparation of graphene oxide (GO)

Graphene oxide was synthesized by chemical oxidation in an improved Hummers' method[24]. In brief, 500 mg of graphite flakes was added into the mixture of concentrated H₂SO₄/H₃PO₄ (60 : 6.7 ml). Then, 3.0 g KMnO₄ was slowly added with vigorous stirring producing a slight exotherm to 35~40 °C. The mixture solution was stirred vigorously about 12 h maintaining the temperature of 323 K. The reaction was then cooled to room temperature and poured into the 400 ml ice with 1.5 ml of 35% hydrogen peroxide aqueous solution. Afterwards, the dispersion was filtered, washed

with 200 ml water, HCl and absolute ethanol in succession and finally dried under vacuum condition. The NH₂-graphene was obtained via a hydrothermal method with ethylenediamine[25]. Typically, a certain amount of GO was added into the ethanol solution (50 ml) ultrasonication for 1 h forming with a homogeneous suspension. The ethylenediamine solution was dropped into the suspension subsequently (pH=12.5) under vigorous stirring. The solution was then sealed in Teflon-lined stainless-steel autoclave and placed in an oven at 160 °C for 24 h, and then was cooled to room temperature naturally. The precipitate was collected and washed with deionized water. The yielded product was dried at 80 °C in air for further use.

The bulk-MnO₂ were synthesized in a reported method[26]. In a typical reaction, 20 ml of a pre-blended solution of 0.6 M tetramethylammonium hydroxide (TMA·OH) and 30 wt% hydrogen peroxide was added into 10 ml of 0.3 M MnCl₂·4H₂O aqueous solution within 15 s. The solution turned dark brown immediately, showing the evidence that Mn²⁺ was stirring vigorously for 12 h at room temperature. Afterwards, the precipitate was washed with water and methanol and dried in a vacuum oven at 60 °C. In our case, the layered H-type birnessite MnO₂ and NH₂-graphene can be exfoliated by water and DMF solution. Then, the two solution were mixed and sealed in a teflon lined stainless autoclave and heated at 160 °C for 8 h. The resulting product were washed thoroughly with deionized water and ethanol and dried at 60 °C in oven.

2.3 Adsorption experiment

The Cr⁶⁺ was used as an objective pollutant to evaluate the adsorptive performance of the as-prepared materials. Analytical grade potassium dichromate was used to prepare the 1000 mg/l stock solution, which was further diluted to the required concentration before use. To investigate the adsorption capacity of the different adsorbents. 0.02 g different materials were added into 100 ml of a 300 mg/l Cr⁶⁺ solution at a fixed pH of 2.0. For the equilibrium, the initial Cr⁶⁺ concentration were varied in the range of 50-300 mg/l. After a specified time, the fixed amounts of the suspension were withdrawn and filtered by 0.45 μm membrane filter for further analysis.

The pH effect experiments were performed at the initial Cr⁶⁺ concentration of 300 mg/l by adjusting the initial pH in the range of 2.0-11.0 using 0.1 mol/l HCl and

NaOH. Kinetic studies were conducted using 0.1 g α -MnO₂-NH₂-RGO in 500 ml of the adsorbent solution (100 mg/l, 200 mg/l, 300 mg/l). Thermodynamic tests were performed at different temperatures (275 K, 298 K, 328 K) with various solution ranging from 50 mg/l to 300 mg/l. The adsorb amount was calculated as follows:

$$q_e = \frac{(c_0 - c_e)v}{m}$$

Where q_e is the amount of Cr⁶⁺ adsorbed by the as-prepared materials (mg/g) at any time (t); c_0 is the initial Cr⁶⁺ concentration (mg/l); c_t is the Cr⁶⁺ concentration after a fixed time (mg/l), v is the sample volume (l) and m is the weight of the adsorbents (g). For the regeneration, 0.02 g of α -MnO₂-NH₂-RGO was first added into 100 ml of 300 mg/l Cr⁶⁺ solution in 150 min. After adsorption, we separated the adsorbents with high speed centrifugation, washed with distilled water several times, and the adsorbents were immersed in 100 ml of 0.1 M NaOH solution for 150 min. Before the second adsorption, the adsorbent was treated by 0.1 M HCl solution for 150 min. Regenerated α -MnO₂-NH₂-RGO were used for adsorption in the five cycles.

3. Results and discussion

3.1 Characterization of different materials

Fig.1 showed the typical XRD pattern of GO, NH₂-RGO, bulk-MnO₂ and α -MnO₂-NH₂-RGO, conforming the ultrathin sheets structure of α -type MnO₂ on the NH₂-graphene. As can be seen that the most intensive peak of GO at around $2\theta = 9.8^\circ$ was in corresponding with the (001) reflection, and the interlayer spacing (0.91 nm) was much larger than that of graphite (0.34 nm) because of the introduction of oxygen-containing functional groups on the pristine graphite sheets[27,28]. The diffraction peaks of NH₂-RGO (25°) explained that the GO was reduced by ethylenediamine. The weak broad peaks of bulk-MnO₂ around 12.23° , 37.8° , 63.64° , corresponding to the (001), (101), and (110) crystal planes of δ -MnO₂ showed a low degree of crystallinity. The α -MnO₂-NH₂-RGO nanocomposite corresponded to the (110), (200), (310), (211), (411) and (521) crystal planes of α -MnO₂[29].

Hydrothermal treatment facilitated the phase transition from δ -MnO₂ to α -MnO₂. These finds are well consistent with the MnO₂ crystal growth theory[30,31].

The FTIR spectra were investigated to affirm the process for the preparation of α -MnO₂-NH₂-RGO hybrids. In the case of GO, the characteristic peaks appeared at 3416 cm⁻¹ and 1408 cm⁻¹ were assigned to the O-H stretching and bending vibration of inter-calated water. The absorption bands of oxygen groups at 1228 cm⁻¹, 1624 cm⁻¹ and 1738 cm⁻¹ were ascribed to the C-OH/C-O-C groups, and carbonyl moieties, C=O stretching of the -COOH, respectively[32]. While in the FT-IR spectrum of NH₂-RGO and α -MnO₂-NH₂-RGO, the amplitudes of the oxygen-containing functional characteristic bands decrease to a great degree, or the peaks even disappeared. It revealed that the GO was reduced after the hydro-thermal treatment. In addition, the new peaks located at 1583 cm⁻¹ of NH₂-RGO and α -MnO₂-NH₂-RGO was ascribed to stretching vibration of N-H (in the C-NH group)[33]. Sharp peaks around 600-500 cm⁻¹ were observed which can be attributed to Mn-O and Mn-O-Mn vibration in MnO₆ octahedral[34]. A new peak at around 725 cm⁻¹ was observed in α -MnO₂-NH₂-RGO, which was observed in α -MnO₂-NH₂-RGO, and it was attributed to the bending vibration of the Mn-O-C bond because of the interactional reaction between carbon and MnO₄⁻ ions. The results confirm that an intimate contact exists between graphene and MnO₂[35].

The morphology of the as-prepared materials were investigated by using TEM. Fig. 3a and 3b shows that flake-like shapes of GO with the wrinkles. Fig. 3c and 3d showed that the MnO₂ with sheet-like shape is homogeneously and tightly integrated on the NH₂-graphene surfaces, and the ultrathin MnO₂ sheets have widths ranging from 10 to 30 nm. It can be seen that the graphene sheets with large area and flat morphology served as an ideal microscopic substrates to host the α -MnO₂ nanosheets (Fig. 3d) to a maximum areal utilization. Furthermore, the existence of NH₂-RGO, MnO₂ in the nanocomposite has been testified by the peaks of C, N, Mn, and O in the EDX analysis as exhibited in Fig. 3e.

According to the N₂ adsorption-desorption isotherms (Fig. 4) of the GO, NH₂-RGO, bulk MnO₂ and α -MnO₂-NH₂-RGO. It conformed to the type-IV curves with an H₃

hysteresis loop, and the shapes indicated meso- and macro-porous characteristics[36]. From the Table 1, it can be seen that the α -MnO₂-NH₂-RGO composite had a higher specific surface area (117 m²/g) than that of the GO (41 m²/g), NH₂-RGO (57 m²/g), but lower than the bulk MnO₂ (212 m²/g), because the bulk MnO₂ was analyzed without exfoliated. The results indicated that MnO₂ ultrathin sheets were dispersed on the surface of the NH₂-RGO, which can present the aggregation of graphene sheets[35]. The α -MnO₂-NH₂-RGO showed a mesoporous structure with an average pore size of 14.256 nm. The high specific surface area and mesoporous structure of α -MnO₂-NH₂-RGO make them very promising candidates for the sorption of Cr(VI) in the wastewater.

3.2 Adsorption capacity of different materials

The adsorption amount of different nanocomposites were discussed, and the results were presented in Fig. 5. The adsorption capacity of NH₂-RGO was greater than that of GO, indicating that the amino groups on the NH₂-RGO were expected to be the active centers for Cr⁶⁺. The adsorption amount of bulk-MnO₂ is higher than that of GO, because manganese oxides have larger surface area and have higher affinities than GO. The α -MnO₂-NH₂-RGO nanocomposites were the most effective removal materials compared with the others, because more binding sites were provided. MnO₂ loading level on the surface of NH₂-RGO was suitable for Cr⁶⁺ adsorption, and the morphology of α -MnO₂ was uniform and thin and more binding sites were provided. Thus, the adsorption amount of different nanocomposites primarily relied on the functional groups, as well as on the morphology of adsorbent surface.

3.3 Effect of the pH on Cr⁶⁺ adsorption

Adjustment of the initial Cr⁶⁺ pH value is a crucial parameter, which dominated the adsorption process particularly the adsorption capacity. This parameter caused the change of the surface charge of the adsorbent, transformation of the chromium species and other ions present in the solution and degree of dissociation of functional groups on the active sites of the sorbent[37]. From the Fig.S8, We can clearly see that the XRD without any change. So we think that the composite has the stability under the condition of strong acid. Fig. 6 exhibit that the Cr⁶⁺ sorption capacity decreases with

the increase in pH from 2.0 to 11.0. The Cr^{6+} species may be represented in aqueous solution primarily as HCrO_4^- and $\text{Cr}_2\text{O}_7^{2-}$ were the predominant species with a pH lower than 6.8, and CrO_4^{2-} was prime form of Cr^{6+} when pH is above 6.8[38,39]. The uptake of hexavalent chromium at lower pH indicated that the pro-dominant component (HCrO_4^-) of Cr^{6+} necessitated one exchange site from the $\alpha\text{-MnO}_2\text{-NH}_2\text{-RGO}$ in order to occur for the adsorption. On the contrary, at high pH, the divalent forms of Cr^{6+} ($\text{Cr}_2\text{O}_7^{2-}$, CrO_4^{2-}) were almost excited and needed two adsorption sites from the $\alpha\text{-MnO}_2\text{-NH}_2\text{-RGO}$ to occur for the adsorption[37]. Thus, the adsorption amount of $\alpha\text{-MnO}_2\text{-NH}_2\text{-RGO}$ was much larger at lower pH than that at higher pH. Furthermore, the amino groups in $\alpha\text{-MnO}_2\text{-NH}_2\text{-RGO}$ occurred the protonation and deprotonation due to the interaction mechanism. The reaction in Eq.(1) illustrated that the protonation of amino groups enhanced at low solution pH, making the $\alpha\text{-MnO}_2\text{-NH}_2\text{-RGO}$ surface to be more positive charged, leading to the binding of anionic Cr^{6+} species strongly. With increasing solution pH, the ability of -NH_2 to be protonated weakened, and OH^- ions may be adsorbed to the surface of the adsorbent through hydrogen bonds leading to more coulombic repulsion of metals[40]



Where Sur denoted the surface of $\alpha\text{-MnO}_2\text{-NH}_2\text{-RGO}$. In addition, the chromium was an active metal, and the binding of Cr^{6+} with the $\alpha\text{-MnO}_2\text{-NH}_2\text{-RGO}$ may be resulted from the partial conversion of hexavalent chromium to the reduced speciation of trivalent chromium. The reduction of Cr^{6+} into Cr^{3+} by reducing substrate (CxOH) on the occurrence of redox reactions between the surface groups and the Cr^{6+} at low pH values[41,42]



In order to affirm that Cr^{3+} coexists with Cr^{6+} , we measured the concentration of total chromium and found that Cr^{3+} exists in the solution. Hydroxyl and carboxyl groups

in adsorbents are suspected to bind Cr^{3+} ions by surface complexation and cation exchange mechanisms[41].

In brief, the adsorption of Cr^{6+} is a complicated process, and the mechanism includes electrostatic attraction, complexation ion exchange and so forth[43].

3.4 Adsorption isotherm

Adsorption isotherms are the mathematical models that describe the solid-liquid adsorption system. Based on a set of assumptions, isotherms are primarily related to the homogeneity/ heterogeneity of adsorbents. In addition, the type of coverage and how adsorbate could interact with adsorbent are involved. The experimental adsorption equilibrium data were fitted on the langmuir, Freundlich and Du-Radushkevich (D-R) isotherms to represent adsorption equilibrium. Fig. 7. shows the adsorption isotherms for Cr^{6+} on the surface of $\alpha\text{-MnO}_2\text{-NH}_2\text{-RGO}$ at different temperatures. The Langumir model is derived from several assumptions, such as the uniform energies of adsorption site and no transmigration of adsorbate on the surface of materials. The model takes the following linear form[44]:

$$\frac{1}{q_e} = \frac{1}{q_m} + \frac{1}{q_m b c_e}$$

$$R_L = \frac{1}{1 + bC_0}$$

Where q_e (mg/g) was the adsorption capacity at an equilibrium state on adsorbent q_m and b (l/mg) signified the maximum adsorption amount and the apparent energy of the adsorption, respectively. C_e and C_0 (mg/l) represent the equilibrium concentration and initial concentration of Cr^{6+} , respectively (Fig. S1). The R_L value can demonstrated whether the isothermal type is favorable ($0 < R_L < 1$) or unfavorable ($R_L > 1$). The Freundlich isotherm which is appreciable to heterogeneous surfaces and multilayer adsorption, which is defined as follows [45]:

$$\ln q_e = \frac{1}{n} \ln c_e + \ln K_F$$

Where K_F (mg/g (l/mg)^{1/n}) and n signified the adsorption capacity and the adsorption intensity, respectively. The Freundlich constants K_F and $1/n$ were obtained from the

slop and intercept of the equation process (Fig. S2). The D-R isotherm was applied to estimate the mean free energy of adsorption (E) in order to confirm the process is physical adsorption or chemical adsorption. Dubinin and Radushkevich [46] have proposed that the adsorption occurs on a single uniform pore. In this connection, the D-R isotherm is used extensively, because the assumption do not contain the homogeneous surface or similar adsorption energy[47].

$$\ln q_e = \ln q_m - \beta \varepsilon^2$$

$$\varepsilon = RT \ln\left(1 + \frac{1}{c_e}\right)$$

Where β (mol^2/kJ^2) is a constant related to sorption mean free energy and ε is the polony potential (Fig. S3). The mean free energy of adsorption can be calculated out using the following relationship:

$$E = \frac{1}{\sqrt{2\beta}}$$

From Table 2, we can see that the hexavalent Cr^{6+} ions were favorably adsorbed on the $\alpha\text{-MnO}_2\text{-NH}_2\text{-RGO}$, and the adsorption amount of Cr^{6+} obtained was 333 mg/g, 350 mg/g, 371 mg/g at 275 K, 298 K and 328 K. The sorption amount attained with the $\alpha\text{-MnO}_2\text{-NH}_2\text{-RGO}$ was much higher than that gained with many other reported adsorption. In consideration of the correlation coefficient as a criterion for goodness of fit for the adsorption process, the Frenudlich isothermal adsorption exhibited the better correlation ($R^2=0.996, 0.993, 0.997$) than the Langmuir ($R^2=0.924, 0.928, 0.933$) and D-R ($R^2=0.81, 0.85, 0.84$) isothermal model, which demonstrated that the Frenudlich isothermal adsorption system more ideally. Table 2 indicates that the adsorption of Cr^{6+} is a multi-adsorption process, because Frenudlich isothermal adsorption model assumes a multilayer adsorption and the stronger binding sites are occupied first by the adsorbates[48]. Furthermore, the K_F and n were calculated from Fig. S2. The value of K_F is 34.33, 45.84, 55.26, while n is 2.5, 2.8, 2.98. The n can be used to predict the adsorption characteristics. For $n < 1$ the adsorption is unfavorable, n between a value of 1 and 2 adsorption is defined as moderately

difficult with the value of n between 2 and 10 is considered good adsorption[49]. The n determined in our studies represents good adsorption that were in accordance with the larger value of K_F . The parameter E (kJ/mol) indicated the adsorption mechanism, which is physical or chemical. If the magnitude of E is between 8 and 16 kJ/mol, the adsorption process occurs chemically, while the value of $E < 8$ kJ/mol corresponds to a physical adsorption process[50,51]. From the calculated value of the mean free adsorption energy, it indicated that the adsorption mechanism of Cr^{6+} on the $\alpha\text{-MnO}_2\text{-NH}_2\text{-RGO}$ may be a physical adsorption. However, D-R isotherm was poorly fitted to the adsorption process with regression coefficient. Combining with the reference of pseudo second order kinetics, it could suggest that the adsorption process may be occurred by a physical-chemical mechanism[52].

3.5 Adsorption kinetics

The kinetics of adsorption on the $\alpha\text{-MnO}_2\text{-NH}_2\text{-RGO}$ about different initial Cr^{6+} concentration in Fig. 8. Possible mechanisms can be investigated in accordance with several reaction processes such as chemical reaction, diffusion control and mass transport kinetics. Pseudo-first-order model, pseudo-second-order model and the intraparticle diffusion model were employed to analyze the kinetics of Cr^{6+} adsorption. The pseudo-first-order model is expressed by the equation as[53]

$$\lg(q_e - q_t) = \lg q_e - \frac{k_1}{2.303} t$$

Where q_e and q_t represented the amount of Cr^{6+} adsorbed (mg/g) at the equilibrium time and time t (min), respectively. k_1 (min^{-1}) is the rate constants (Fig. S4). The pseudo-second-order rate equation is given as[54]

$$\frac{t}{q_t} = \frac{1}{k_2 q_e^2} + \frac{t}{q_e}$$

Where k_2 was the pseudo-second-order rate constants, q_e , q_t and t had the same definitions as those in the pseudo-first-order kinetics equation (Fig. S5). The initial adsorption rate h (mg/g/min)[55] as follows:

$$h = k q_e^2$$

The intra-particle diffusion model is given as [56]

$$q_t = k_p t^{0.5} + c$$

Where k_p was the intraparticle diffusion rate constant ($\text{mg/g}/\text{min}^{1/2}$). The kinetic parameters under different conditions are listed in Table 3. The correlation coefficient (R^2) of pseudo-second order model (0.993, 0.995, 0.994) was much higher than the pseudo-first order model (0.85, 0.94, 0.946), and the calculated value of q_e from the pseudo-second-order model (209 mg/g , 261 mg/g , 346 mg/g) fitting were in accordance with the experimental ones (194 mg/g , 256 mg/g , 334 mg/g). This results indicated that the adsorption conforms to the pseudo-second-order reaction mechanism, and the reaction rate of the whole adsorption process is controlled by chemical adsorption rather than mass transfer[57]. The initial adsorption rate increased with an increase in initial Cr^{6+} concentration, possibly because a more efficient utilization of the adsorption capacity of the adsorbent was expected at higher initial concentration due to the greater driving force[58]. When the linear plots of q versus $t^{0.5}$ passing through the origin, the intraparticle diffusion play a significant role in the sole rate-limiting. Intra-particle diffusion from the solid-liquid interface to the interior of the solid particle played a significant role in Cr^{6+} adsorption onto the surface of $\alpha\text{-MnO}_2\text{-NH}_2\text{-RGO}$. When the linear plots of q vs. $t^{0.5}$ passing through the origin, the intra-diffusion was the sole rate-limiting process. Fig. 9 shows that the intraparticle diffusion is not the only rate-limiting step, although it is involved in the adsorption, and boundary layer diffusion also has an effect of adsorption to some level.

3.6 Thermodynamic studies

The thermodynamic parameters provide in-depth information about internal energy changes that are associated with adsorption. The adsorption standard Gibbs free energy changes (ΔG°), the average standard enthalpy change (ΔH°), and the standard entropy change (ΔS°) can be obtained from the thermodynamic equilibrium constant K_0 with the change of temperature on the Cr^{6+} adsorption onto $\alpha\text{-MnO}_2\text{-NH}_2\text{-RGO}$ to evaluate the adsorption process. K_0 is calculated as follows[59]:

$$K_0 = \frac{a_s}{a_e} = \frac{v_s C_s}{v_e C_e} \quad (1)$$

Where a_s was the activity of the adsorbed Cr^{6+} , a_e is the activity of the Cr^{6+} at equilibrium, C_s (mmol/g) was the capacity of Cr^{6+} adsorbed per $\alpha\text{-MnO}_2\text{-NH}_2\text{-RGO}$ mass, C_e (mmol/ml) was the equilibrium concentration, v_s is the activity coefficient of the adsorbed Cr^{6+} , and v_e was the activity coefficient of Cr^{6+} in solution. As the concentration of the Cr^{6+} approaches unity, reducing Eq. (1) to the following form

$$\frac{C_s}{C_e} = \frac{a_s}{a_e} = K_0 \quad (2)$$

The K_0 were obtained by plotting $\ln(C_s/C_e)$ versus C_s and extrapolating C_s to zero (Fig. S6). The adsorption standard Gibbs free energy changes (ΔG°) can be obtained:

$$\Delta G^\circ = -RT \ln K_0$$

Where R was the gas constant (8.314 kJ/mol/k), T was the absolute temperature in Kelvin. The values of ΔH° , ΔS° for Cr^{6+} adsorption were obtained from slop and intercept of linear plot of $\ln K_0$ versus $1/T$ (Fig. S7) using the following equations[60]

$$\ln K_0 = \frac{\Delta S^\circ}{R} - \frac{\Delta H^\circ}{RT}$$

The thermodynamic parameters were listed in Table 4. The negative values of ΔG° demonstrate that the adsorption process was spontaneous. In addition, with increased temperature, the ΔG° value becomes more negative, revealing that higher temperature facilitated the spontaneity due to a greater driving force of adsorption or activation of the adsorbent surface[61]. The calculated ΔG° values suggest that the adsorption process was primarily a physical process. However, chemical adsorptions may also occur, because the calculated value of ΔG° range 20 kJ/mol to 80 kJ/mol, which is the process that physical-adsorption combines with the chemical adsorption. The obtained result was in good agreement with the result found with the D-R isotherm. The positive value of ΔH° revealed that the interaction of Cr^{6+} adsorbed by $\alpha\text{-MnO}_2\text{-NH}_2\text{-RGO}$ was endothermic process. The positive cause was that the metal ions are well hydrated and will need breaking of the hydration bind to facilitate

adsorption, which consequently requires higher energy. Thus, higher temperature accelerate the dehydration process. The positive standard change (ΔS°) suggested an increased disorder at the solid-solution interface[62].

3.7 Regeneration of α -MnO₂-NH₂-RGO

From a practical/industrial point view, the recycling and the reuse of the adsorbent is an economic necessity. Taking into account that the nanocomposites showed a poor adsorption ability at high pH, alkaline condition treatment is likely to be a suitable method for the regeneration of α -MnO₂-NH₂-RGO. Thus, a 0.1 M NaOH solution was used, and the adsorption-desorption cycles were replicated five times using same batch of α -MnO₂-NH₂-RGO (Fig.10). The as-prepared composite still exhibited more than 81% adsorption capacities after five cycles of reuse, indicating that α -MnO₂-NH₂-RGO have the good regeneration and reusability for Cr⁶⁺ adsorption. This was consistent with the above result that higher pH depressed the adsorption of Cr⁶⁺, but was beneficial to its recovery.

3.8 Adsorption mechanism

The Cr⁶⁺ sorption of the α -MnO₂-NH₂-RGO primarily might occur via the electrostatic attraction route in the early stage, whereas it became chemical adsorption via the covalent bonding route in the late stage[26]. In aqueous solution, Cr⁶⁺ ions exist in the form of Cr₂O₇²⁻, HCrO₄⁻, et., the amine groups on the sorbent were protonated in order to form surface complexes with the chromium species via electrostatic attraction which explains the pH effect on the adsorption (Fig. 6). Moreover, the foremost sorption group was MnO₂, because the sorption amount of α -MnO₂-NH₂-RGO was better than that of NH₂-RGO(Fig. 5). The MnO₂ was amphoteric and can feature with weak acid or weak base characteristics. The protonation and deprotonation of oxide surface was controlled by the pH of the Cr⁶⁺ solution. Therefore, when the pH was low, the MnO₂ could be efficiently protonated form = MnOH with a positive charge[63], and an anion HCrO₄⁻ could thus be bound through electrostatic attraction. In addition, the redox reactions may proceed either sequentially and /or in parallel, especially in the acidic condition. Furthermore, it would be occur an ion exchange between Cr₂O₇²⁻, HCrO₄⁻, and the OH⁻ on

α -MnO₂-NH₂-RGO generating the ion exchange and so on constitute the adsorption mechanism[64].

3.9 Comparison of adsorbent performance with literature data

To evaluate the effectiveness of α -MnO₂-NH₂-RGO as a potential adsorption for Cr (VI), the maximum adsorption capacity q_m was compared with those of other adsorbents reported previously. The maximum adsorption amount of α -MnO₂-NH₂-RGO were higher than the values of graphene/MgAl, monodisperse Fe₃O₄, iron nanoparticle decorated graphene, Fe₃O₄-graphene, and several surface-modified MnO₂ nanoparticles such as MnO₂, manganese oxide nanofibers, MnO₂-modified expanded graphite, MnO₂ nanowires-diatomite, and MnO₂/Fe₃O₄/o-MWCNTs, but lower than Polyethyleneimine- graphene oxide (GO) and UV-active functionalized-graphene oxide. Compared to the MnO₂, manganese oxide nanofibers, MnO₂-modified expanded graphite and MnO₂/Fe₃O₄/o-MWCNTs, the α -MnO₂-NH₂-RGO displayed a higher area, which could provide more adsorption active sites. Moreover, the crystallization of MnO₂ thin film on the surface of RGO also generated more active oxygen, and the resultant interface contributed to the excellent adsorption. Moreover, introducing the functional groups, especially metal oxide and amino groups can enhance the adsorption capacity and dispersion of graphene. It is worth noting that α -MnO₂-NH₂-RGO is very stable under acid conditions. For the above reasons, α -MnO₂-NH₂-RGO can be considered as a promising adsorbent for the effective removal of Cr (VI).

4. Conclusion

In summary, we have fabricated for the first time a novel, high-performance adsorbent by chemically integrating α -MnO₂ nanosheets on NH₂-graphene due to the strong electrostatic interaction. The results exhibited that the adsorption capacity depended on the pH strongly and initial Cr⁶⁺ concentration, the adsorption data were found to fit well with the Freundlich isotherm model. The adsorption equilibrium was achieved within 100 min, and the maximum adsorption capacity was 371 mg/g. The adsorption kinetics were found to follow the pseudo-second-order equation. By calculating the

thermodynamic parameters, it indicated that the adsorption process was spontaneous and exothermic. The D-R model showed that sorption had physical-chemical nature. The adsorption capacity of α -MnO₂-NH₂-RGO can remain up to 81% after five cycles of usage. The results obtained in this study illustrated that the α -MnO₂-NH₂-RGO is expected to be an effective and economically adsorbent for Cr(VI) removal from aqueous system.

Acknowledgment

We thank classmates for giving many suggestions on this work.

Notes and references

^a College of Chemistry and Chemical Engineering, Lanzhou University, Lanzhou 730000, PR China.

^b College of Life Science, Lanzhou University, Lanzhou 730000, PR China.

^c Address here.

* Please direct correspondence to yansq@lzu.edu.cn. Tel. /fax: +86 931 8912582.

Electronic Supplementary Information (ESI) available: [details of any supplementary information available should be included here]. See

DOI: 10.1039/b000000x/

References

- [1] J. Johnson, L. C. Wel, A. E. Graedel, *Environ. Sci. Technol.* 40 (2006) 7060-7069.
- [2] Y. P. Huang, H. Ma, S. G. Wang, M. W. Shen, R. Guo, X. Y. Cao, M. F. Zhu, and X. Y. Shi, *ACS. Appl. Mater. Interf.* 4 (2012) 3054-3061.
- [3] W. J. Jiang, M. Pelaez, D. D. Dionysiou, M. H. Entezari, D. Tsoutsou, K. O'Shea, *Chem. Eng. J.* 222 (2013) 527-533.
- [4] K. G. Bhattacharyya and S. S. Gupta, *Ind. Eng. Chem. Res.* 45 (2006) 7232-7240.
- [5] D. H. Thomas, J. S. Rohrer, P. E. Jackson, T. Pak, J. N. Scott, *J. Chromatogr. A* 956 (2002) 255-259.
- [6] S. Rengaraj, C. K. Joo, Y. H. Kim, J. Yi, *J. Hazard. Mater. B.* 102 (2003) 257-275.
- [7] N. M. Lee, H. Carlsson, H. Aspegren, T. Welander and B. Andersson, *Water. Sci. Technol.* 34 (1996) 101-109.
- [8] A. Hafez, S. El-Manharawy, *Desalination* 165 (2004) 141-151.
- [9] D. Zhang, S. Y. Wei, C. D. Kaila, X. Su, J. Wu, A. B. Karki, D. P. Young and Z. H. Guo, *Nanoscale* 2 (2010) 917-919.
- [10] L. Fan, C. N. Luo, M. Sun and H. M. Qiu, *J. Mater. Chem.* 22 (2010) 24577-24583.
- [11] L. L. Fan, C. N. Luo, M. Sun and H. M. Qiu, *J. Mater. Chem.* 22 (2012) 24577-24583.
- [12] P. Y. Dong, Y. H. Wang, L. N. Guo, B. Liu, S. Y. Xin, J. Zhang, Y. R. Shi, W. Zeng and S. Yin, *Nanoscale* 4 (2012) 4641-4649.
- [13] K. P. Loh, Q. L. Bao, P. K. Ang and J. X. Yang, *J. Mater. Chem.* 20 (2010) 2277-2289.
- [14] J. W. Qin, M. H. Cao, N. Li and C. W. Hu, *J. Mater. Chem.* 21 (2011) 17167-17174.
- [15] X. Y. Yan, X. L. Tong, Y. F. Zhang, X. D. Han, Y. Y. Wang, G. Q. Jin, Y. Qin and X. Y. Guo, *Chem. Commun.* 48 (2012) 1892-1894.

- [16] B.J. Li, H. Q. Cao and G. Yin, *J. Mater. Chem.* 21 (2011) 13765-13768.
- [17] M. Willander, K. U. Hasan, O. Nur, A. Zainelabdin, S. Zaman and G. Amin, *J. Mater. Chem.* 22 (2012) 2337-2350.
- [18] B. J. Li, H. Q. Cao, G. Yin, Y. X. Lu and J. F. Yin, *J. Mater. Chem.* 21 (2011) 10645-10648.
- [19] Y. H. Xue, H. Chen, D. S. Yu, S. Y. Wang, M. Yardeni, Q. B. Dai, M. M. Guo, Y. Liu, F. Lu, J. Qu and L. M. Dai, *Chem. Commun.* 47 (2011) 11689-11691.
- [20] E. J. Kim, C. S. Lee, Y. Y. Chang, and Y. S. Chang, *ACS. Appl. Mater. Interf.* 5 (2013) 9628-9634.
- [21] R. P. Han, W. H. Zou, H. K. Li, Y. H. Li, J. Shi, *J. Hazard. Mater. B* 102 (2006) 934-942.
- [22] R. P. Han, W. H. Zou, Z. P. Zhang, J. Shi, J. J. Yang, *J. Hazard. Mater. B* 137 (2006) 384-395.
- [23] Z. W. Zhao, J. Liu, F. Y. Cui, H. Feng and L. L. Zhang, *J. Mater. Chem.* 22 (2012) 9052-9057.
- [24] D. C. Marcano, D. V. Kosynkin, J. M. Berlin, A. Sinitskii, Z. Z. Sun, A. Slesarev, L. B. Alemany, W. Lu and J. M. Tour, *ACS. Nano.* 4 (2010) 4806-4814.
- [25] L. Zhang, H. Z. Li, Y. Liu, Z. Tian, B. Yang, Z. B. Sun and S.Q. Yan, *RSC Adv.* 4 (2014) 48703-48711.
- [26] L. L. Peng, X. Peng, B. R. Liu, C. Z. Wu, Y. Xie, and G. H. Yu, *Nano. Lett.* 13 (2013) 2151-2157.
- [27] S. Chen, J. W. Zhu, X. D. Wu, Q. F. Han and X. Wang, *ACS. Nano.* 4 (2010) 2822-2830.
- [28] C. Xu, X. D. Wu, J. W. Zhu, X. Wang, *Carbon* 46 (2007) 386-389.
- [29] JCPDS 00-044-0141
- [30] Y. C. Du, G. W. Zheng, J. S. Wang, L. P. Wang, J. S. Wu, H. X. Dai, *Micro. Mes. Mater.* 200 (2014) 27-34.
- [31] X. L. Huang, N. T. Hu, R.G Gao, Y. Yu, Y. Y. Wang, Z. Yang, E. Siu, W. Kong, H. Wei and Y. F. Zhang, *J. Mater. Chem.* 22 (2012) 22488-22495.

- [32] Y. Liu, R. J. Deng, Z. Wang and H. T. Liu, *J. Mater. Chem.* 22 (2012) 13619-13624.
- [33] A. B. Yuan, Q. L. Zhang, *Electrochem. Commun.* 8 (2006) 1173-1178.
- [34] M. C. Hu, K.S. Hui, K.N. Hui, *Chem. Eng. J.* 254 (2014) 237-244.
- [35] G. D. Jiang, Z. F. Lin, C. Chen, L. H. Zhu, Q. Chang, N. Wang, W. Wei, H. Q. Tang, *Carbon* 49 (2011) 2693-2701.
- [36] M. S. Hosseini, A. H. Bandegharaei, H. Raissi, F. Belador, *J. Hazard. Mater.* 169 (2009) 52-57.
- [37] L. Tang, Y. Fang, Y. Pang, G. M. Zeng, J. J. Wang, Y. Y. Zhou, Y. Y. Deng, G. D. Yang, Y. Cai, J. Chen, *Chem. Eng. J.* 254 (2014) 302-312.
- [38] Y. Pang, G. M. Zeng, L. Tang, Y. Zhang, Y. Y. Liu, X. X. Lei, Z. Li, J. C. Zhang, Z. F. Liu, Y. Q. Xiong, *Chem. Eng. J.* 175 (2011) 222-227.
- [39] A. M. Yusof, N. A. N. N. Malek, *J. Hazard. Mater.* 162 (2009) 1019-1024.
- [40] Q. Q. Zhong, Q. Y. Yue, B. Y. Gao, Q. Li, X. Xu, *Chem. Eng. J.* 229 (2013) 90-98.
- [41] J. Hu, C. L. Chen, X. X. Zhu, X. K. Wang, *J. Hazard. Mater.* 162 (2009) 1542-1550.
- [42] G. R. Xu, J. N. Wang, C. J. Li, *Chem. Eng. J.* 198-199 (2012) 310-317.
- [43] J. Anandkumar, B. Mandal, *J. Hazard. Mater.* 168 (2009) 633-640.
- [44] A. Kurniawan, H. Sutiono, N. Indraswati, S. Ismadji, *Chem. Eng. J.* 189-190 (2012) 264-274.
- [45] M. Brdar, M. Šćiban, A. Takači, T. Došenović, *Chem. Eng. J.* 183 (2012) 108-111.
- [46] N. D. Hutso and R. T. Yang, *Adsorption*, 3 (1997) 189-195.
- [47] N. Ünlü, M. Ersoz, *J. Hazard. Mater.* 136 (2006) 272-280.
- [48] S. Haider, S. Y. Park, *J. Membr. Sci.* 328 (2009) 90-96.
- [49] M. Atienza-Martínez, I. Fonts, J. Ábrego, J. Ceamanos, G. Gea, *Chem. Eng. J.* 222 (2013) 534-545.
- [50] I. Kiran, T. Akar, A. S. Ozcan, A. Ozcan, S. Tunalı, *Biochem. Eng. J.* 31 (2006) 197-203.

- [51] M. S. Onyango, Y. Kojima, O. Aoyi, E. C. Bernardo, H. Matsuda, J. Col. Interf. Sci. 279 (2004) 341-350.
- [52] F. Raji, M. Pakizeh, Appl. Surf. Sci. 282 (2013) 415.
- [53] M. Chairat, S. W. Rattanaphani, J. B. Bremner and V. Rattanaphani, Dyes Pigm. 76 (2008) 435-439.
- [54] Y. S. Ho and G. Mc. Kay, Process Biochem. 34 (1999) 451-465.
- [55] E. Demirbas, N. Dizge, M. T. Sulak, M. Kobya, Chem. Eng. J. 148 (2009) 480-487.
- [56] N. Li, Z. Mei, X. Wei, Chem. Eng. J. 192 (2012) 138-145.
- [57] R. Sitko, E. Turek, B. Zawisza, E. Malicka, E. Talik, J. Heimann, A. Gagor, B. Feist and R. Wrzalik, Dalton. Trans. 42 (2013) 5682-5689.
- [58] Q. Q. Zhong, Q. Q. Yue, Q. Li, B. Y. Gao, X. Xu, Carbohydrate Polymers 111 (2014) 788-796.
- [59] R. Niwas, U. Gupta, A. A. Khan, K. G. Varshney, Colloids and Surfaces A: Physicochemical and Engineering Aspects 164 (2000) 115-119
- [60] L. Ai, C. Y. Zhang, Z. L. Chen, J. Hazard. Mater. 192 (2011) 1515-1524.
- [61] R. P. Han, Z. Lu, W. H. Zou, D. T. Wang, J. Shi, J. J. Yang, J. Hazard. Mater. 137 (2006) 480-488.
- [62] M. Bhaumik, A. Maity, V. V. Srinivasu, M. S. Onyango, J. Hazard. Mater. 190 (2011) 381-390.
- [63] R. P. Han, W. H. Zou, Z. P. Zhang, J. Shi, J. J. Yang, J. Hazard. Mater. B 137 (2006) 384-395.
- [64] X. F. Sun, Y. Ma, X. W. Liu, S. G. Wang, B. Y. Gao, X. M. Li, Water Res. 44 (2010) 2517-2524.
- [65] X. Y. Yuan, Y. F. Wang, J. Wang, C. Zhou, Q. Tang, X. B. Rao, Chem. Eng. J. 221 (2013) 204-213.
- [66] V. Linsha, P. S. Suchithra, A. P. Mohamed, S. Ananthakumar, Chem. Eng. J. 220 (2013) 244-253.
- [67] C. V. Gherasim, G. Bourceanu, Chem. Eng. J. 220 (2013) 24-34.

- [68] C. Noubactep, K. B. D. Btatkeu, J. B. Tchatchueng, *Chem. Eng. J.* 178 (2011) 78-84.
- [69] A. H. Qusti, *J. Ind. Eng. Chem.* 20 (2014) 3394-3399.
- [70] Y. B. Liu, Y. Q. Wang, S. M. Zhou, S. Y. Lou, L. Yuan, T. Gao, X. P. Wu, X. J. Shi, and K. Wang, *ACS. Appl. Mater. Interf.* 4 (2012) 4913-4920.
- [71] H. Y. Jin, J. Yuan, H. Y. Hao, Z. J. Ji, M. Liu, S. Hou, *Mater. Lett.* 110 (2013) 69-72.
- [72] H. Jabeen, V. Chandra, S. Jung, J. W. Lee, K. S. Kim and S. B. Kim, *Nanoscale* 3 (2011) 3583-3585.
- [73] C. Luo, Z. Tian, B. Yang, L. Zhang, S. Q. Yan, *Chem. Eng. J.* 224 (2013) 256-265.
- [74] H. Jabeen, V. Chandra, S. Jung, J. W. Lee, K. S. Kim and S. B. Kim. *Nanoscale* 3 (2011) 3583-3585.
- [75] J. H. Chen, H. T. Xing, H. X. Guo, W. Weng, S. R. Hu, S. X. Li, Y. H. Huang, X. Sun and Z. B. Su, *J. Mater. Chem. A*, 2 (2014) 12561-12570.
- [76] D. Dinda, A. Gupta and S. K. Saha, *J. Mater. Chem. A* 1 (2013) 11221-11228.

Fig.1. XRD patterns of GO, NH₂-RGO, bulk-MnO₂, α -MnO₂-NH₂-RGO.

Fig.2. FTIR spectra of GO, NH₂-RGO, bulk-MnO₂, α -MnO₂-NH₂-RGO.

Fig.3. TEM image of (a) GO (b) NH₂-RGO (c, d) α -MnO₂-NH₂-RGO (e) δ -MnO₂ sheets (f) EDX pattern of α -MnO₂-NH₂-RGO.

Fig.4. Nitrogen sorption isotherms for (1) bulk-MnO₂ (2) α -MnO₂-NH₂-RGO (3) NH₂-RGO (4) GO.

Fig.5. Adsorption capacity of different materials for Cr⁶⁺.

Fig.6. Effect of the pH on Cr (VI) adsorption on the α -MnO₂-NH₂-RGO.

Fig.7. Adsorption isotherms for Cr⁶⁺ on the surface of α -MnO₂-NH₂-RGO at different temperatures.

Fig.8. The kinetics of adsorption on the α -MnO₂-NH₂-RGO about different initial Cr⁶⁺ concentration.

Fig.9. Weber-Morris plots for the kinetic modeling of Cr⁶⁺ adsorbed onto α -MnO₂-NH₂-RGO at different temperatures.

Fig.10. The regeneration of α -MnO₂-NH₂-RGO for Cr⁶⁺ adsorption.

Table 1. Pore characteristics of GO, NH₂-RGO, bulk-MnO₂, α -MnO₂-NH₂-RGO.

Table 2 Parameters of the Langmuir, Freundlich and D-R isotherms for Cr⁶⁺ adsorption onto α -MnO₂-NH₂-RGO.

Table 3. Kinetic parameters for Cr⁶⁺ adsorption onto α -MnO₂-NH₂-RGO.

Table 4. Thermodynamic parameters for Cr⁶⁺ adsorption onto α -MnO₂-NH₂-RGO.

Table 5 Maximum adsorption capacities of Cr⁶⁺ on α -MnO₂-NH₂-RGO and other adsorbents.

Fig.1

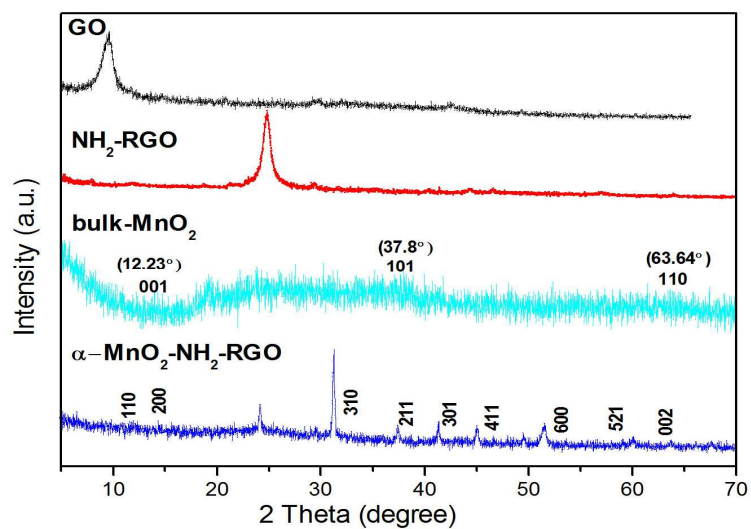


Fig.2

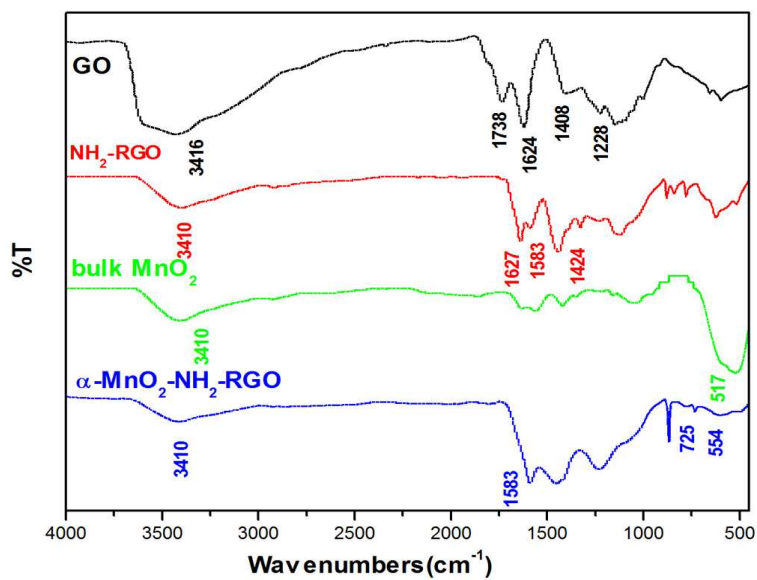


Fig.3

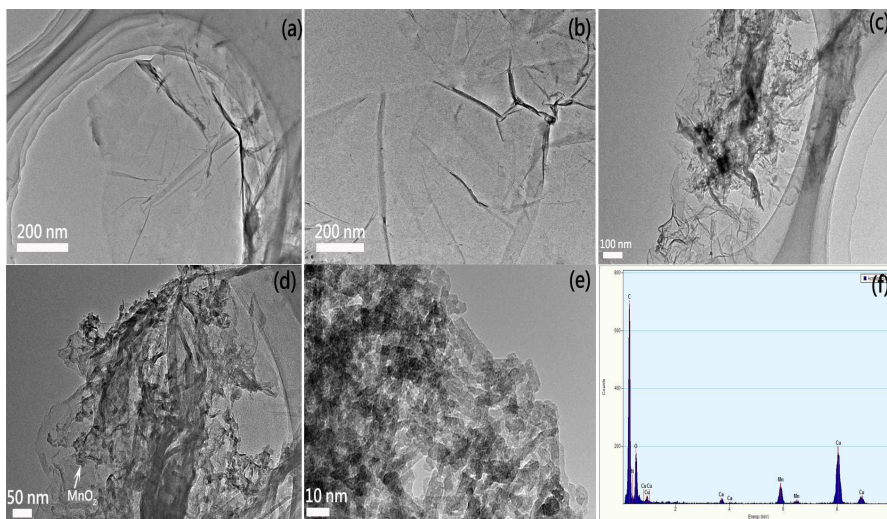


Fig.4

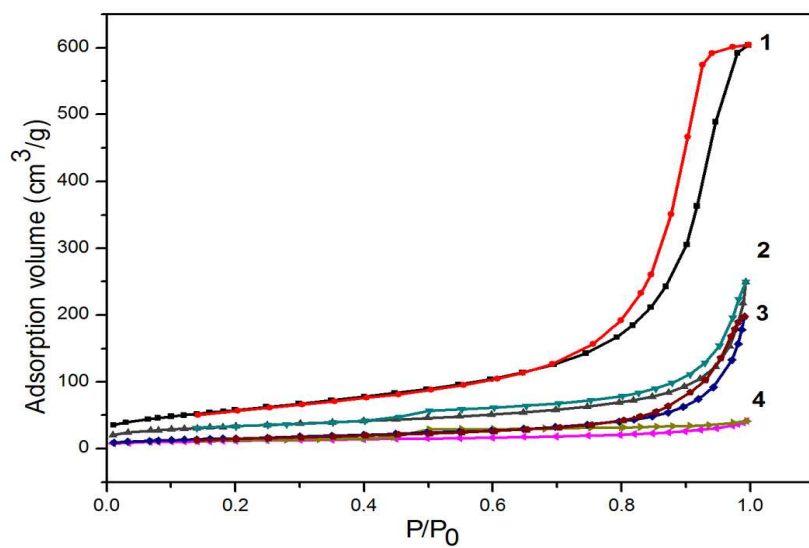


Fig.5

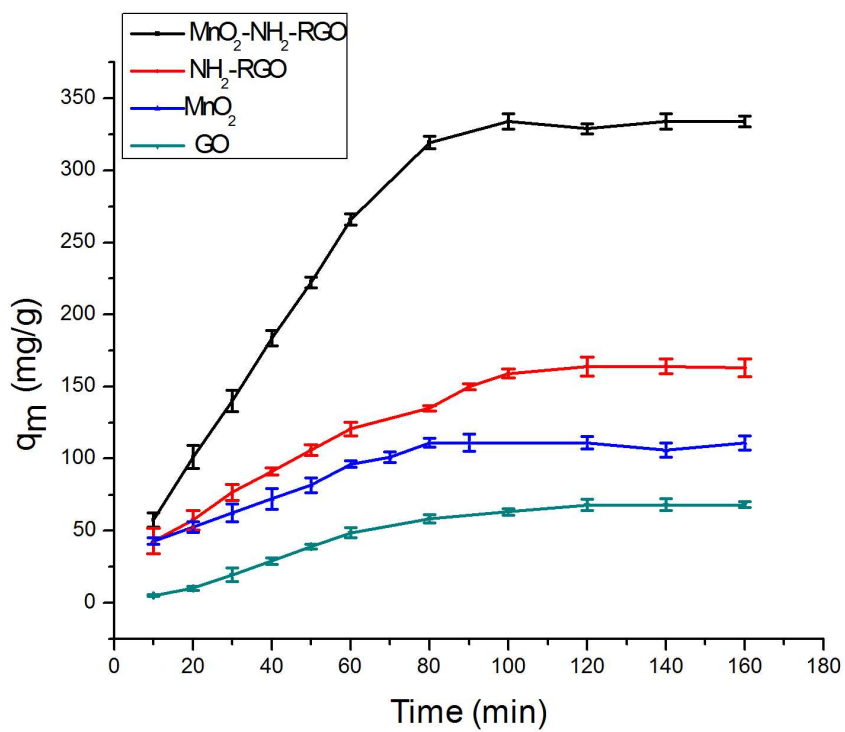


Fig.6

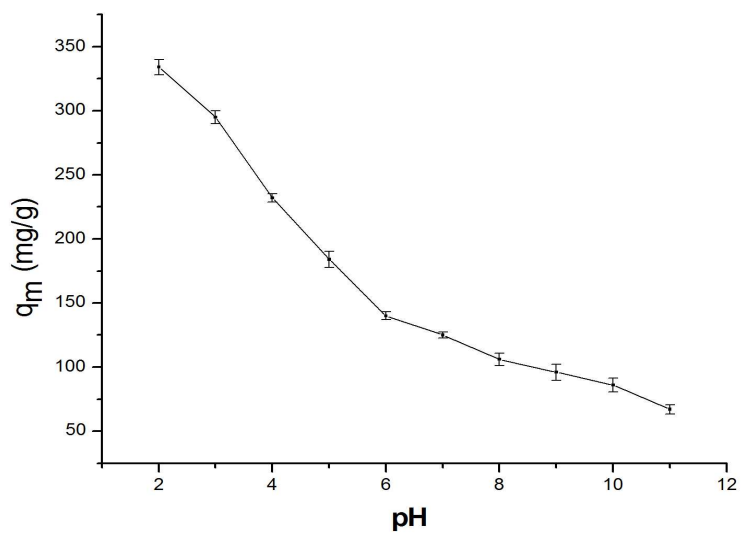


Fig.7

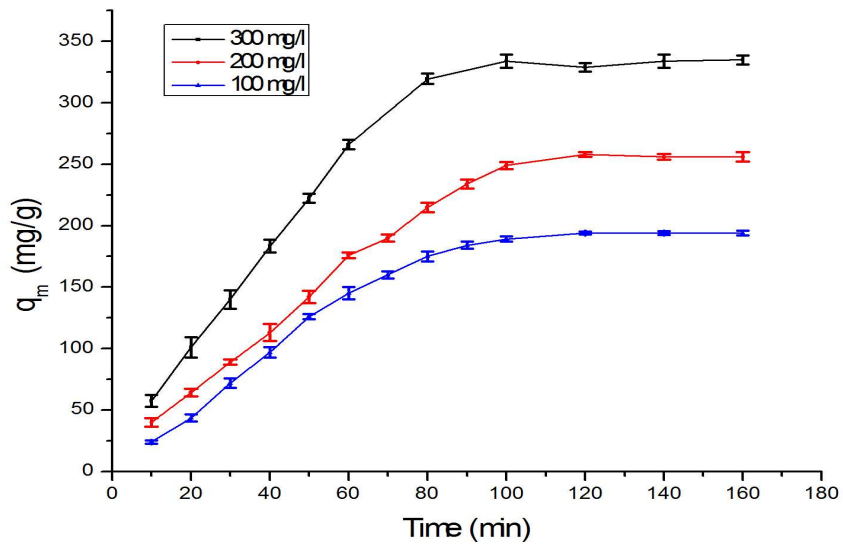


Fig.8

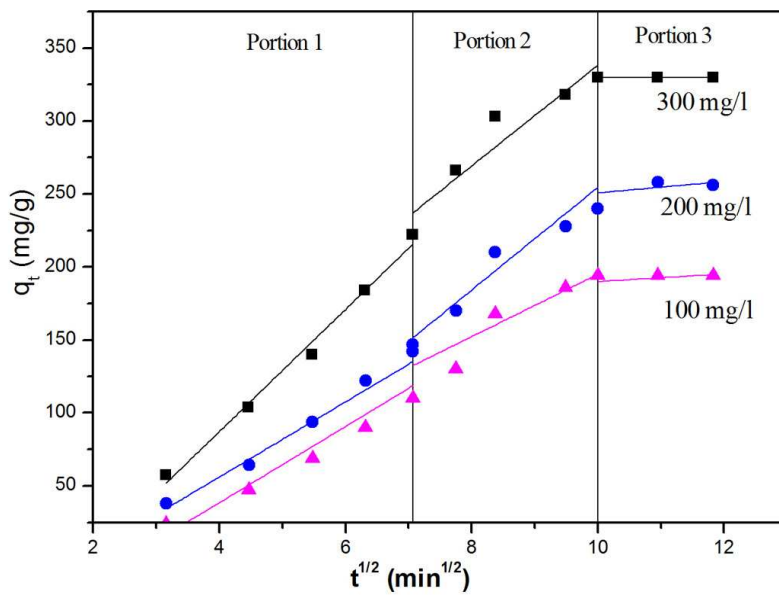


Fig.9

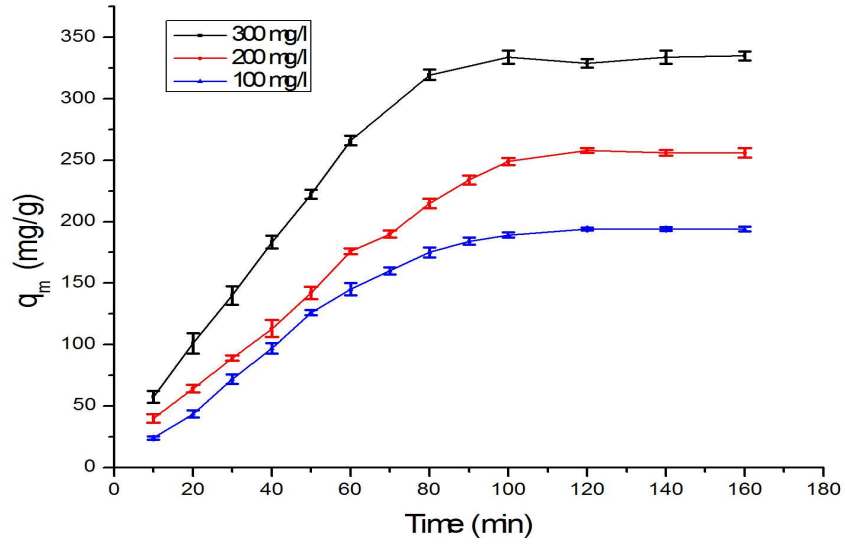


Fig.10

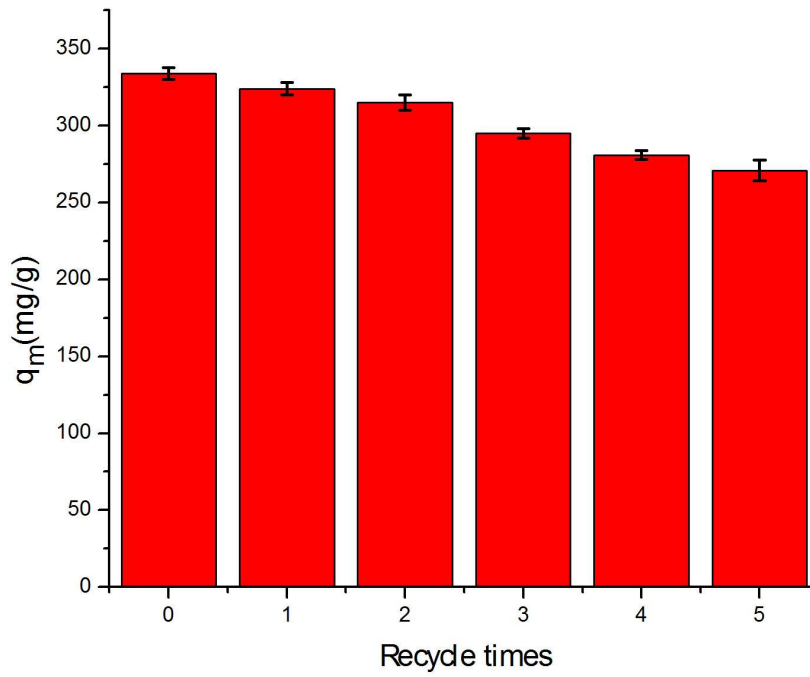


Table 1

Materials	Surface area (m ² /g)	Pore Volume (cm ³ /g)	Pore size (nm)
GO	40.76	0.07435	5.2689
NH ₂ -RGO	57.16	0.3165	20.965
bulk-MnO ₂	211.97	1.03948	14.537
α -MnO ₂ -NH ₂ -RGO	117.59	0.3904	14.256

Table 2

T(K)	Langmuir isotherm				Freundlich isotherm			D-R isotherm			
	q_m	b	r_1^2	R_L	n	K_F	r_2^2	q_m	β (mol ² /J ²)	E (J/mol)	r_3^2
275	333	0.0306	0.924	0.417-0.106	2.5	34.33	0.996	257	7.61×10^{-5}	81	0.81
298	350	0.0298	0.928	0.402-0.1	2.8	45.84	0.993	284	6.27×10^{-5}	89	0.85
328	371	0.0405	0.933	0.331-0.076	2.98	55.26	0.997	302	3.97×10^{-5}	112	0.84

Table 3

C ₀ (mg/l)	q _{e,exp}	Preudo-first-order kinetic model			Preudo-second-order kinetic model			
		k ₁	q _e	r ₁ ²	k ₂	q _e (×10 ⁻⁴)	h	r ₂ ²
100	194	0.0303	275	0.85	1.20	209	5.24	0.993
200	256	0.026	325	0.94	1.23	261	8.38	0.995
300	334	0.0352	398	0.95	1.32	346	15.8	0.994

Table 4

T (K)	$\ln K_0$	ΔG° (kJ/mol)	R^2	ΔH° (kJ/mol)	ΔS° (J/mol/K)	R^2
275	9.525	21.78	0.969			
298	9.746	24.15	0.991	6.73	103.7	0.996
328	10.01	27.29	0.992			

Table 5

Adsorbates	Adsorbents	q_{\max} (mg/g)	Refs.
Cr ⁶⁺	Calcined graphene/MgAl layered double hydroxides	177.6	[65]
	Amine-grafted alumino-siloxane hybrid	48.96	[66]
	40% Aliquat 336/60% PVC PIM	50.85	[67]
	MnO ₂	51.996	[68]
	Manganese oxide nanofibers	11.8	[69]
	High saturation magnetization monodisperse Fe ₃ O ₄ hollow microsphere	180	[70]
	MnO ₂ -modified expanded graphite	0.3011	[71]
	Iron nanoparticle decorated graphene	162	[72]
	MnO ₂ nanowires in situ grown on diatomite	197.6	[30]
	MnO ₂ /Fe ₃ O ₄ /o-MWCNTs	186.9	[73]
	Graphene oxide	65.2	[10]
	Iron nanoparticle decorated graphene	162	[74]
	Polyethyleneimine- graphene oxide (GO)	539.5	[75]
	UV-active functionalized-graphene oxide	393.8	[76]
α -MnO ₂ -NH ₂ -RGO	371	Present work	